Journal of Materials Chemistry A

ROYAL SOCIETY OF CHEMISTRY

COMMUNICATION

View Article Online
View Journal | View Issue

Cite this: J. Mater. Chem. A, 2025, 13, 12097

Received 11th December 2024
Accepted 28th March 2025

DOI: 10.1039/d4ta08811e

rsc.li/materials-a

Suppressing the penetration of 2D perovskites for enhanced stability of perovskite solar cells†

Xinran Xu, [ab] Zhuoqiong Zhang,[c] Tanghao Liu,*[a] Pengchen Zhu,[d] Zhipeng Zhang*[e] and Guichuan Xing *[e]

In recent years, perovskite solar cells (PSCs) have shown rapid development, bringing them closer to commercialization. Surface passivation has proven critical in enhancing device performance due to the higher defect density at the film surface compared to the bulk. Introducing 2D perovskite layers is a widely adopted passivation strategy; however, the penetration of large organic cations into the underlying 3D perovskite layer can hinder charge transport and damage the film structure. In this work, we modified the commonly used ammonium salt PEAI by introducing fluorine atoms at various positions on the benzene ring (*o*-FPEAI, *m*-FPEAI, and *p*-FPEAI) and investigated their effects on passivation and stability. Our results show that *m*-FPEAI effectively inhibits the penetration of the 2D phase, improving charge transport and device stability due to a strong steric effect. Photoluminescence (PL) and transient absorption (TA) spectroscopy confirmed that *m*-FPEAI-treated films exhibited superior suppression of non-radiative recombination and enhanced stability under ambient conditions. Devices incorporating *m*-FPEAI achieved a maximum power conversion efficiency (PCE) of 24.63% and retained over 80% of their initial efficiency after 1750 hours of continuous illumination. This study demonstrates the critical role of fluorine positioning in optimizing surface passivation and offers valuable insights for further improving PSC performance and stability.

Introduction

In the past decade, perovskite solar cells (PSCs) have achieved remarkable development, with certified efficiencies now reaching 27%, showing great potential for commercialization.[1–7] Various techniques, including composition engineering, interface engineering, passivation engineering, *etc.*, have been developed to boost their performance.[8–13] Among these, surface passivation has proven critical, as defect densities are significantly higher at the film surface than in its interior.[14] The introduction of a 2D perovskite modification layer has been widely recognized as an effective passivation strategy for several reasons.[15,16] Firstly, the amino group can passivate lead dangling bonds through interactions between its lone pair of electrons and the perovskite. This interaction helps reduce the density of electronic trap states at the surface. Secondly, the hydrophobic nature of large cations plays a crucial role in protecting the perovskite films from moisture-induced degradation. Thirdly, the introduction of 2D perovskite as a modification layer could regulate the interfacial-energy-level alignment between perovskite and adjacent layers and facilitate charge separation. Lastly, the incorporation of a 2D layer at the interface acts as a barrier inhibiting ion migration across the layers, enhancing the operational stability of the device.[10,17–19]

Generally, a 2D layer is formed by coating a solution of large organic ammonium salt onto the perovskite film surface. However, during this process, large cations may penetrate into the underlying 3D perovskite layer, damaging the structure of the film and impeding charge transport. This penetration triggers the formation of a 2D phase within the 3D layer, which compromises the structural and electronic integrity of the 3D perovskite and causes a loss of efficiency to some extent. Therefore, suppressing interfacial diffusion between the 2D and 3D layers is highly desirable.[20–22]

To address this issue, Jiang *et al.* developed a transfer-imprinting-assisted growth method, which uses the solid-state transfer technique to deposit the 2D layer onto the 3D layer.[23] This solution-free method effectively avoids interfacial diffusion. However, it requires additional imprinting steps, which require careful optimization of heat and pressure. In comparison, suppressing the reaction between large-cation salts and

[a]School of Physical Sciences, Great Bay University, Dongguan, 523000, China. E-mail: tanghaoliu@gbu.edu.cn

[b]Department of Physics, Hong Kong Baptist University, Hong Kong SAR, 999077, China

[c]Department of Applied Physics, Hong Kong Polytechnic University, Hong Kong SAR, 999077, China

[d]School of Sustainable Energy and Resources, Nanjing University, Suzhou, 215163, China

[e]Joint Key Laboratory of the Ministry of Education, Institute of Applied Physics and Materials Engineering, University of Macau, Avenida da Universidade, Taipa, Macau SAR, 999078, China. E-mail: zhipengzhang@um.edu.mo; gcxing@um.edu.mo

† Electronic supplementary information (ESI) available. See DOI: https://doi.org/10.1039/d4ta08811e

the 3D perovskite through modifications to the salts themselves offers a simpler and more practical approach. In this work, we modified the widely used ammonium salt, phenylethylammonium iodide (PEAI), by introducing fluorine (F) at different positions on the benzene ring and studied the influence of F location on interfacial diffusion. Our findings reveal that *m*-FPEAI effectively suppresses the penetration of the 2D perovskite phase, leading to improved charge transport and enhanced device stability, which is primarily attributed to its strong steric effects. Photoluminescence (PL) and transient absorption (TA) spectroscopy demonstrated that the *m*-FPEAI-modified films exhibit significantly reduced non-radiative recombination and remarkable stability under ambient conditions. PSCs incorporating *m*-FPEAI achieved an impressive maximum power conversion efficiency (PCE) of 24.63% and retained over 80% of their initial efficiency after 1750 hours of continuous illumination. This work highlights the critical role of fluorine positioning in optimizing surface passivation and provides valuable insights for advancing the performance and stability of PSCs.

Results and discussion

The molecular structures of PEAI and *o*/*m*/*p*-FPEAI are presented in Fig. 1, illustrating the impact of fluorine atom positioning on the molecular properties of these compounds. The position of the fluorine (F) atom plays a crucial role in determining both the molecular size and steric hindrance. These structural variations significantly influence the diffusion behavior of the molecules into the 3D perovskite layer. Among these fluorinated derivatives, *m*-FPEAI exhibited the largest steric hindrance due to its unique molecular configuration, which effectively limited its penetration into the 3D perovskite layer. This restricted diffusion behavior is a key factor in its enhanced device performance, as it prevents excessive intermixing with the 3D phase, thereby preserving the structural integrity and stability of the perovskite film.

The photoluminescence (PL) spectra of the perovskite films were measured and are shown in Fig. 2a and b. To investigate carrier recombination kinetics, we compared the PL intensity of the control (CT) film with those of films treated with PEAI, *o*-FPEAI, *m*-FPEAI, and *p*-FPEAI. The steady-state PL intensity of the perovskite film treated with PEAI was comparable to that of the CT film, indicating minimal differences in non-radiative recombination for these samples. However, the PL intensities of the perovskite films treated with *o*-FPEAI, *m*-FPEAI, and *p*-FPEAI were significantly enhanced, suggesting a substantial reduction in non-radiative recombination. This improvement highlights the critical role of fluorine (F) incorporation in passivating defects and mitigating non-radiative recombination pathways within the perovskite films. The presence of fluorine likely strengthens the chemical interactions at the grain boundaries and interfaces, leading to improved emission properties. The PL intensity of *o*-FPEAI- and *p*-FPEAI-treated films increased by about 20% compared to the CT film, while the PL intensity of the *m*-FPEAI-treated film increased by 60% compared to the CT film. This indicates that non-radiative recombination is most effectively suppressed in the *m*-FPEAI-treated film, possibly due to *m*-FPEAI not being able to penetrate the film. As a result, these molecules remain primarily on the surface, where the trap density is highest. By localizing at the surface, they effectively passivate defects and reduce trap-mediated charge recombination, contributing to improved PL emission.

Owing to their long organic chains, 2D perovskites generally exhibit high hydrophobicity. The incorporation of fluorine further improves this hydrophobicity, which is beneficial for enhancing perovskite stability against moisture. To validate the stability, the surface wettability of different treated perovskite films was evaluated by measuring the water contact angle, as shown in Fig. 2c. After surface treatment with *o*/*m*/*p*-FPEAI, the contact angles of the samples were significantly larger than those of the untreated sample and the PEAI-treated sample. Among them, the *m*-FPEAI-treated sample has the largest contact angle. A larger contact angle indicates greater hydrophobicity, which helps reduce interactions with the external environment and enhances sample stability. To further evaluate ambient stability, the samples were stored in air with a relative humidity (RH) of about 60% and a temperature of about 25 °C. Fig. 2d shows photographs of the samples after 120 days of storage. The CT sample fully degraded to a yellow phase, indicating severe degradation. In contrast, all samples with PEAI and *o*/*m*/*p*-FPEAI modification retained some of their dark phase. Among them, the *m*-FPEAI-modified sample exhibited the largest dark area, confirming its superior stability. X-ray diffraction (XRD) analysis was employed to verify this conclusion. As shown in Fig. 2e, fresh samples showed a sharp peak at 13.9°, which is assigned to the (100) plane of FA-based perovskite. After 120 days, this peak disappeared in the CT sample, confirming complete degradation. For PEAI-, *p*-FPEAI- and *o*-

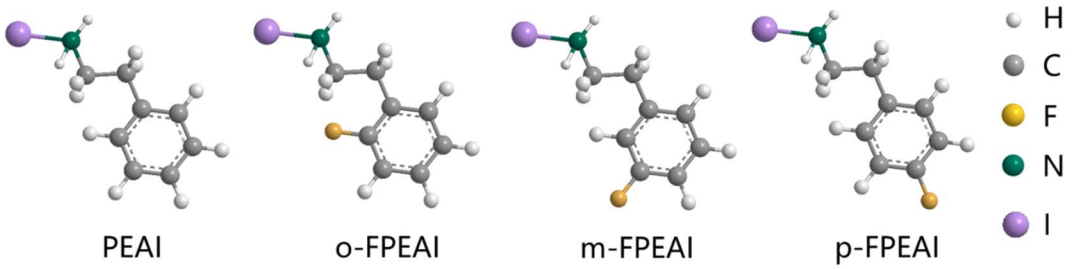

Fig. 1 Molecular structures of PEAI, *o*-FPEAI, *m*-FPEAI, and *p*-FPEAI.

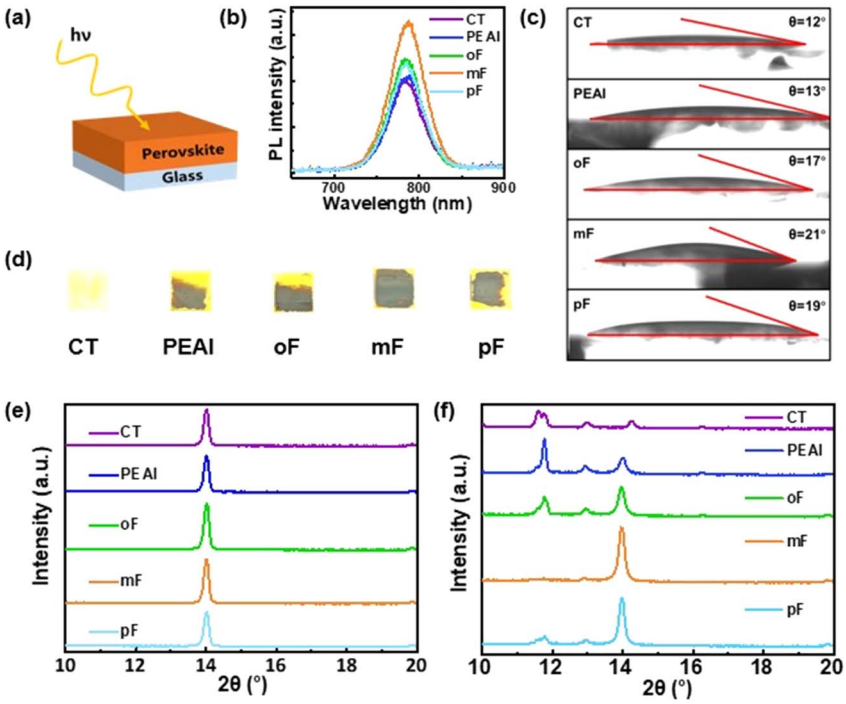

Fig. 2 (a) The structure of the samples used for PL measurement. (b) The PL intensity of the control film, PEAI-treated film, and *o*/*m*/*p*-FPEAI-treated films. (c) Water contact angle measurements of the control perovskite film, PEAI-treated film, and *o*/*m*/*p*-FPEAI-treated film. (d–f) Stability comparison of the control sample, PEAI-treated sample, and *o*/*m*/*p*-FPEAI-treated samples. (d) Visual appearance of the samples after 120 days of storage in air at 25 °C and 60% RH. (e) XRD spectra of the samples prior to storage. (f) XRD spectra of the samples after 120 days of storage.

FPEAI-treated samples, the (100) peak exhibited varying degrees of degradation, as evidenced by the appearance of peaks at 11.8° and 12.6°, which are assigned to δ-$FAPbI_3$ and PbI_2, respectively. In contrast, the *m*-FPEAI-treated sample retained its original diffraction pattern, confirming its superior stability under an ambient atmosphere.

XRD analysis (Fig. S1a†) revealed that perovskite films treated with PEAI, *o*-FPEAI, *m*-FPEAI, and *p*-FPEAI all exhibited a distinct diffraction peak at 5.7°, corresponding to the $(PEA)_2PbI_4$ phase.[10] Additionally, the *o*-FPEAI-treated sample showed an additional peak near 4°, which can be attributed to the $(PEA)_2FAPb_2I_7$ phase.[24] Among the samples, the *m*-FPEAI-treated film exhibited the weakest and least complex 2D diffraction features, suggesting a lower degree of 2D phase formation. XPS analysis in Fig. S1b† further highlighted differences in passivation behavior. The *m*-FPEAI-treated perovskite film exhibited the most pronounced Pb core-level shift, indicating the strongest surface passivation effect. In contrast, other passivation agents (PEAI, *p*-FPEAI, and *o*-FPEAI) showed deeper penetration into the 3D perovskite structure, leading to reactions within the bulk. The Pb core-level shift in the *o*-FPEAI-treated sample was in the opposite direction, aligning with the XRD results, which suggest the formation of a disordered 2D structure. This disorder contrasts with the bulk 2D structural information induced by PEAI and *p*-FPEAI, which may negatively affect film quality.[25] Moreover, Fourier transform infrared spectroscopy (FTIR) analysis in Fig. S1c† reveals that upon introducing *m*-FPEAI, the N–H stretching vibration of FA^+/MA^+ shifted from 3261 cm^{-1} to 3255 cm^{-1} and the C=N stretching vibration of FA^+ shifted from 1710 cm^{-1} to 1706 cm^{-1}. These spectral shifts suggest the formation of hydrogen bonds between *m*-FPEAI and organic cations, contributing to enhanced stability and passivation effects.[25] However, the UV-vis spectra of all perovskite films, as shown in Fig. S2,† appeared nearly identical, indicating that the surface modifications had no significant impact on the absorption properties of the treated films.

Transient absorption (TA) spectroscopy was employed to reveal the phase distribution and charge carrier dynamics in the films. Fig. 3 and S3† display the TA spectra of the various samples. The CT film, without surface modification, showed a single bleaching peak at 765 nm, characteristic of the 3D perovskite phase. In contrast, the other samples showed two dominant bleaching peaks at 555 nm and 765 nm, corresponding to the 2D and 3D phases, respectively.[26] Among these, the *m*-FPEAI-treated film showed the weakest 2D peak, indicating a suppressed 2D phase. The decay curves of the bleaching peak at 765 nm were fitted with multi-exponential models. Perovskite films with PEAI and *o*/*m*/*p*-FPEAI modifications showed much longer carrier lifetimes than the CT perovskite film, as summarized in Table S1.† This improvement is attributed to the passivation of surface defects, a widely reported phenomenon.[10] However, the formation of 2D phases can inhibit charge transfer, and their penetration into the 3D perovskite layer reduces carrier lifetimes. Among these films, the *m*-FPEAI-modified film delivered the longest carrier

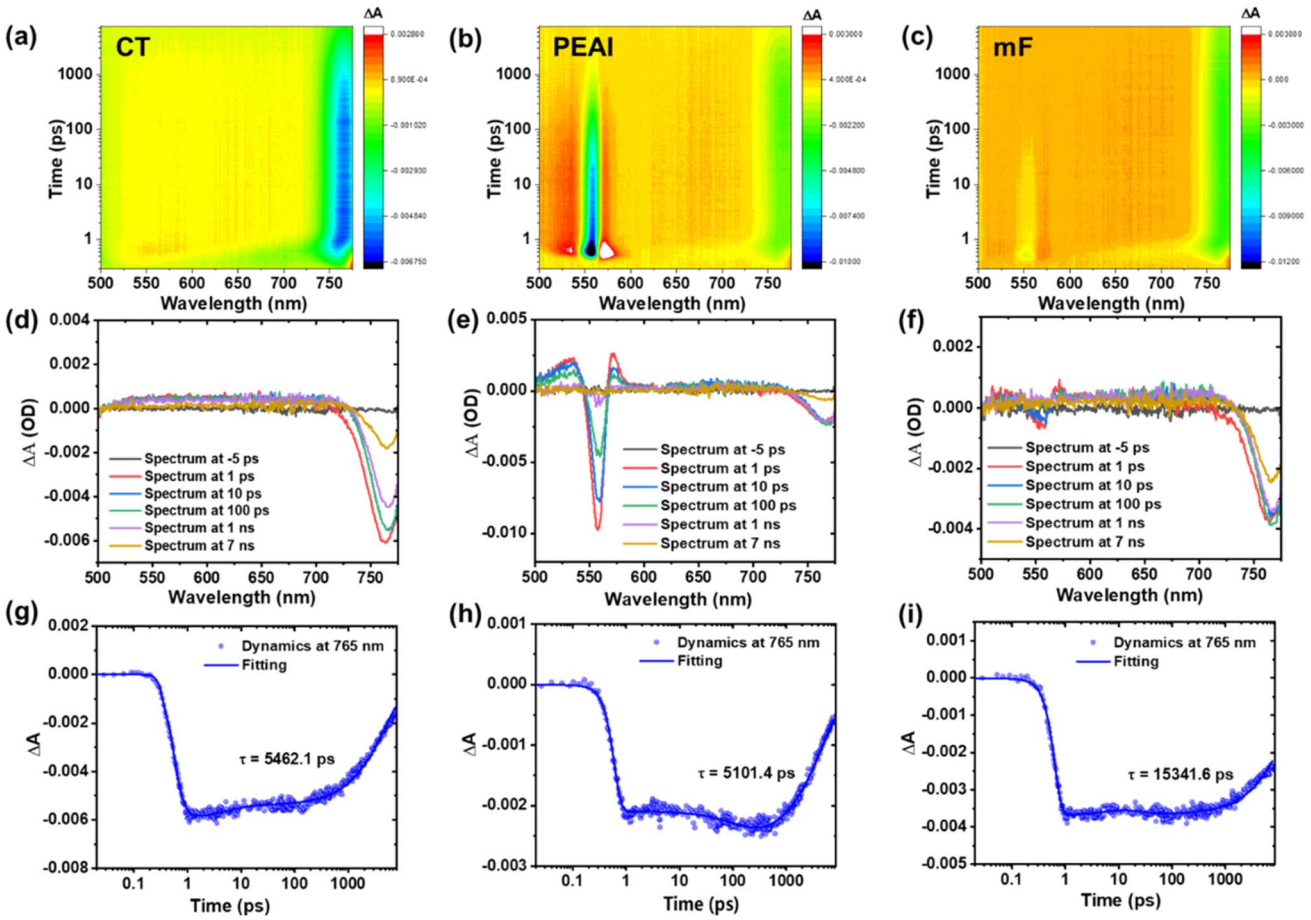

Fig. 3 (a–c) Contour plot TA spectra; (d–f) TA spectra at various decay times; (g–i) decay curves of the bleaching peak at 765 nm for (a, d and g) the control perovskite film and perovskite films modified with (b, e and h) PEAI and (c, f and i) *m*-FPEAI.

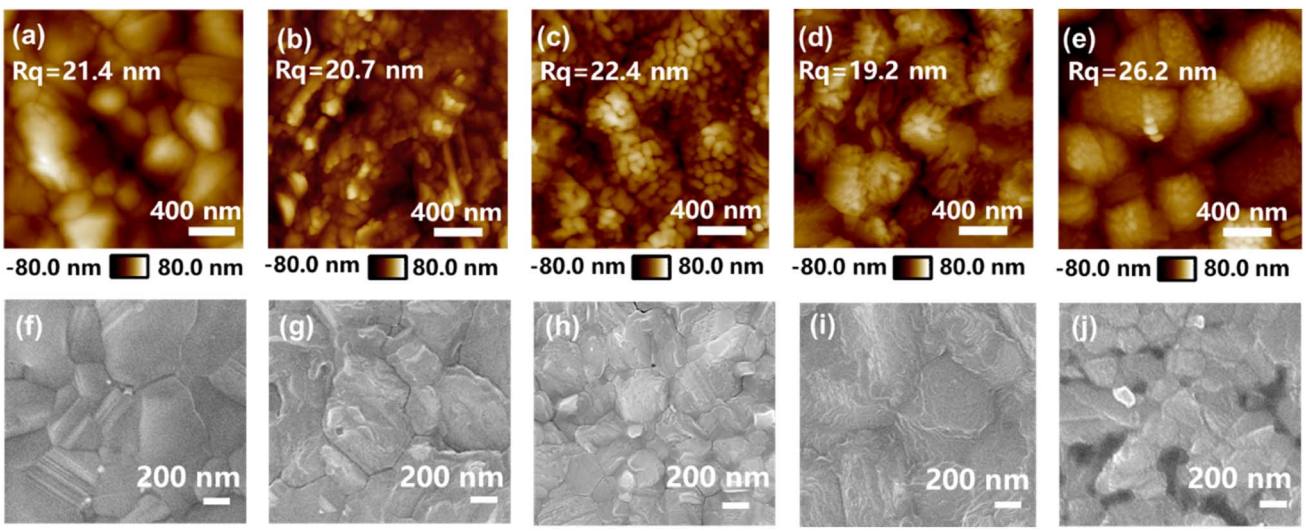

Fig. 4 Surface morphology characterization of perovskite films. (a–e) AFM images of (a) control film, (b) PEAI-treated film, (c) *o*-FPEAI-treated film, (d) *m*-FPEAI-treated film, and (e) *p*-FPEAI-treated film. (f–j) Top-view SEM images of (f) control film, (g) PEAI-treated film, (h) *o*-FPEAI-treated film, (i) *m*-FPEAI-treated film, and (j) *p*-FPEAI-treated film.

lifetime, further confirming the suppressed penetration of 2D phases. In addition, we deposited PEAI and *m*-FPEAI onto the PbI_2 films and explored the formation of 2D perovskites with TA characterization. As shown in Fig. S3,† the 2D signal of the sample with *m*-FPEAI was significantly weaker than that of the PEAI-treated sample. This result indicates that *m*-FPEAI effectively protects the 3D perovskite film by suppressing the formation of 2D phases.

The surface morphology of the perovskite films was investigated with scanning electron microscopy (SEM) and atomic force microscopy (AFM), as shown in Fig. 4. The results showed that all four groups of samples with surface modification exhibited small particles adhering to the surfaces of the perovskite grains. Among the samples, the film modified with *m*-FPEAI displayed the lowest surface roughness and uniform grain size. This enhanced morphology facilitates the formation of ohmic contact with the metal electrode interface, reducing series resistance. SEM images further confirm that PbI_2 crystals are present on the surfaces of the CT, PEAI-treated, and *p*-FPEAI-treated films. These crystals appear as bright regions in the SEM

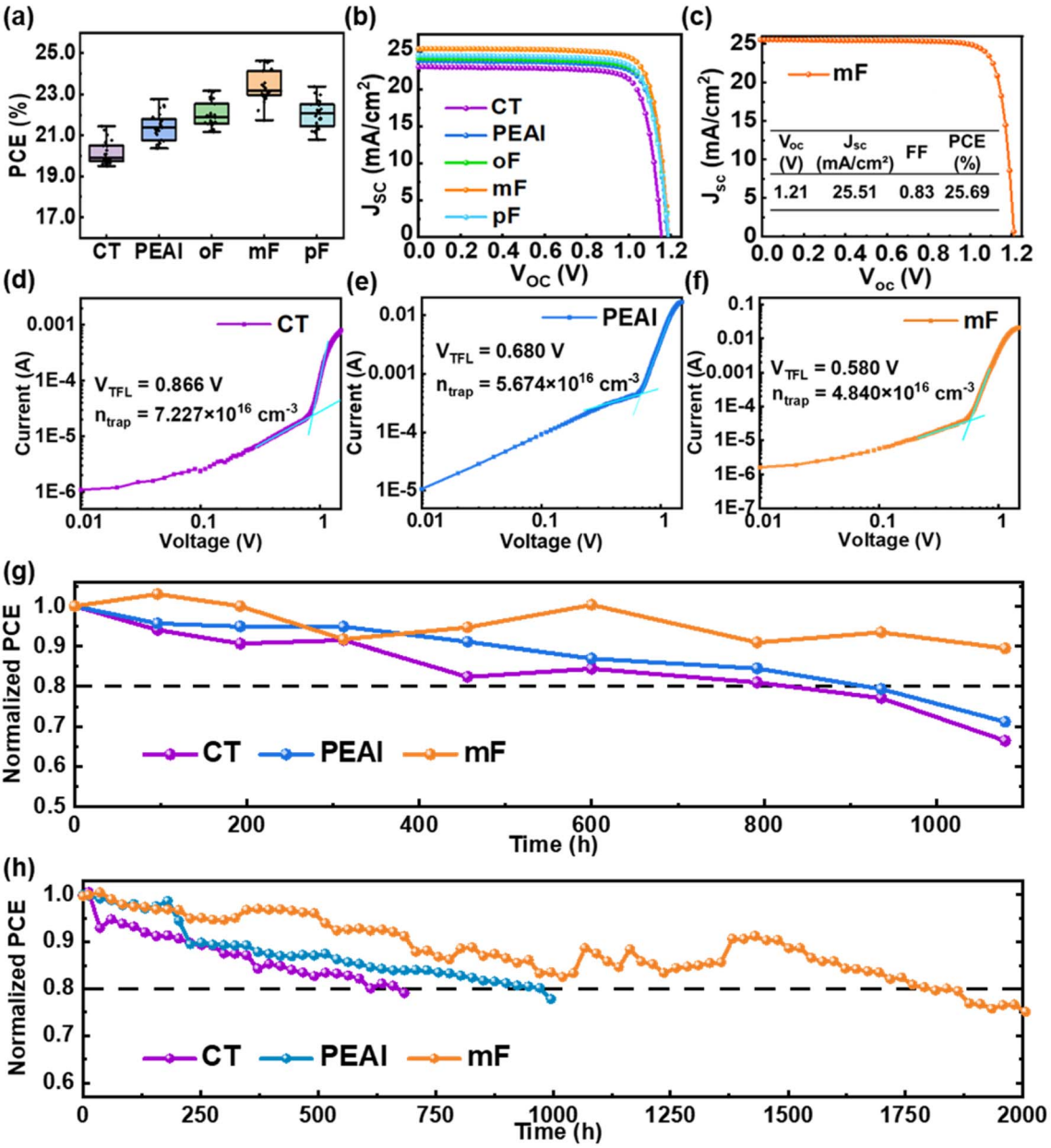

Fig. 5 (a) The photovoltaic-parameter distribution of control PSCs, PEAI-treated PSCs, and *o*/*m*/*p*-FPEAI-treated PSCs with the composition of $Cs_{0.05}FA_{0.88}MA_{0.07}PbI_{2.79}Br_{0.21}$. (b) *J*–*V* characteristics of the control PSC, PEAI-treated PSC, and *o*/*m*/*p*-FPEAI-treated PSCs with the same composition. (c) The best *J*–*V* characteristic of the five groups of PSCs with the composition of $Cs_{0.05}FA_{0.92}MA_{0.03}PbI_{2.91}Br_{0.09}$. (d–f) Space-charge-limited current (SCLC) curves for (d) control PSC, (e) PEAI-treated PSC, and (f) *m*-FPEAI-treated PSC. (g) Normalized PCE evolution during light soaking for the control PSC, PEAI-treated PSC, and *m*-FPEAI-treated PSC under one-sun AM 1.5 G illumination. (h) Maximum power point tracking (MPPT) of normalized power output for control, PEAI-treated, and *m*-FPEAI-treated PSCs under continuous one-sun AM 1.5 G illumination.

micrographs, indicating the accumulation of excess PbI_2 on the film surfaces. Notably, the *p*-FPEAI-treated film exhibits a significantly rougher surface compared to the CT and PEAI-treated films. The SEM images reveal dark, uneven regions on the surface of the *p*-FPEAI-treated film, which can be attributed to increased surface roughness and possible structural damage. This observation suggests that the *p*-FPEAI solution may have a corrosive effect on the perovskite thin film, potentially altering the surface morphology and disrupting the uniformity of the film. In contrast, the SEM image of the *m*-FPEAI-treated film reveals a much smoother and more uniform surface morphology compared to the CT, PEAI-treated, and *p*-FPEAI-treated films. These observations indicate that *m*-FPEAI is more effective in improving the quality of perovskite crystals and may enhance the performance of photovoltaic devices.

Based on the above films, PSCs were fabricated with the structure of ITO/SnO_2/perovskite/spiro-OMeTAD/Au. Their photovoltaic-parameter distributions are shown in Fig. 5a, and representative values are shown in Table 1. Among these devices, the *m*-FPEAI-incorporated PSCs exhibited the highest average PCE of 24.63% as shown in Fig. 5b, primarily attributed to a high short-circuit current density (J_{sc}) of 25.52 mA cm^{-2}. The suppressed formation of 2D phases in the *m*-FPEAI-treated perovskite film, which would otherwise hinder charge transport due to their lower conductivity, facilitated efficient extraction of photo-generated charge carriers. The forward and reverse scan curves in Fig. S6† revealed that the *m*-FPEAI-treated PSCs exhibited the smallest hysteresis among all samples, indicating the most effective defect passivation and improved charge transport. This suggests that *m*-FPEAI not only passivates defects but also suppresses ion migration, enabling more stable and efficient charge extraction. Furthermore, space-charge-limited current (SCLC) measurements (Fig. 5d–f and S7†) confirmed that the *m*-FPEAI-treated perovskite film showed the best carrier transport properties and the lowest defect density. After optimizing the perovskite composition, the PCE of the *m*-FPEAI-treated PSC was further enhanced, reaching 25.69%, as shown in Fig. 5c.

To evaluate the device stability, PSCs were stored under continuous AM 1.5 G illumination and tested every 5 days. As shown in Fig. 5g, only the devices modified with *m*-FPEAI maintained 90% of their initial efficiency after 1080 hours. The devices modified with *o*-FPEAI and *p*-FPEAI surfaces showed slightly better stability than the control group. Additionally, the fluctuation in the stability curves was attributed to the initial oxidation of spiro-OMeTAD, which temporarily enhanced performance before degradation became dominant.[27]

Maximum power point tracking (MPPT) was also tested and is shown in Fig. 5h. After surface modification with *m*-FPEAI, the device exhibited significantly improved long-term stability, maintaining 80% of its initial efficiency after approximately 1750 hours. The consistency between the stability tests further highlights the role of *m*-FPEAI in improving the stability of PSCs. These results further validate the importance of molecular design in optimizing surface passivation strategies, paving the way for the development of more robust and efficient perovskite photovoltaic devices.

Table 1 The representative parameters of the control PSCs, PEAI-treated PSCs, and *o*/*m*/*p*-FPEAI-treated PSCs with the composition of $Cs_{0.05}FA_{0.88}MA_{0.07}PbI_{2.79}Br_{0.21}$

	V_{oc} (V)	J_{sc} (mA cm^{-2})	FF	PCE (%)
CT	1.13	22.43	0.79	19.92
PEAI	1.18	23.33	0.78	21.38
oF	1.18	23.70	0.78	21.93
mF	1.18	24.48	0.80	23.22
pF	1.17	23.58	0.80	22.07

Conclusion

In conclusion, we substituted the widely used PEAI with *o*/*m*/*p*-FPEAI to modify the surface of perovskite films and investigated its effects. Our findings reveal that all *o*/*m*/*p*-FPEAI variants are capable of passivating surface defects on perovskite films, thereby improving their initial performance. However, the position of the fluorine (F) atom on the benzene ring plays a crucial role in determining the extent of penetration into the 3D perovskite layer. A detailed investigation demonstrates that *m*-FPEAI, due to its strong steric effect, effectively minimizes the formation of the 2D phase and preserves the integrity of the 3D layer. As a result, the *m*-FPEAI-based PSC achieved the highest PCE of 24.63%. The champion device maintained over 80% of its initial efficiency after 1750 hours of MPPT testing. This work illustrates the influence of passivator structures on penetration behavior and provides guidance for the further optimization of PSC performance.

Data availability

Data can be obtained from the authors.

Author contributions

X. Xu fabricated the PSCs and prepared the manuscript. Dr Z. Q. Zhang helped in polishing the language. Dr T. Liu designed the materials characterization and helped in preparing the manuscript. Prof. P. Zhu helped analyzing the FTIR and XPS results. Dr Z. P. Zhang and Prof. Xing tested TA spectra, analyzed the results, and prepared the manuscript. All authors agreed with the final version of the manuscript.

Conflicts of interest

There are no conflicts to declare.

Acknowledgements

The authors acknowledge the Science and Technology Development Fund, Macao SAR (File No. FDCT-0082/2021/A2, 0010/2022/AMJ, 0060/2023/RIA1, 0136/2022/A3, 006/2022/ALC, 0122/2024/AMJ, and EF044/IAPME-HG/2022/MUST), UM's research fund (File No. MYRG2022-00241-IAPME, MYRG-GRG2023-

00065-IAPME-UMDF, and MYRG-CRG2022-00009-FHS), the research fund from Wuyi University (EF38/IAPME-XGC/2022/WYU), and the Natural Science Foundation of China (61935017, 62175268, 62288102, and 22405010). X. Xu acknowledges the research platform provided by the Department of Physics, Hong Kong Baptist University. T. Liu acknowledges the start-up grant from Great Bay University.

References

1 N. R. E. Laboratory, *Best Research-Cell Efficiencies*, accesed in Mar. 14, 2025.
2 A. Kojima, K. Teshima, Y. Shirai and T. Miyasaka, *J. Am. Chem. Soc.*, 2009, **131**, 6050–6051.
3 J. Zhou, L. Tan, Y. Liu, H. Li, X. Liu, M. Li, S. Wang, Y. Zhang, C. Jiang, R. Hua, W. Tress, S. Meloni and C. Y. Yi, *Joule*, 2024, **8**, 1691–1706.
4 G. Xing, N. Mathews, S. Sun, S. Lim Swee, M. Lam Yeng, M. Grätzel, S. Mhaisalkar and C. Sum Tze, *Science*, 2013, **342**, 344–347.
5 S. Liu, J. Li, W. Xiao, R. Chen, Z. Sun, Y. Zhang, X. Lei, S. Hu, M. Kober-Czerny, J. Wang, F. Ren, Q. Zhou, H. Raza, Y. Gao, Y. Ji, S. Li, H. Li, L. Qiu, W. Huang, Y. Zhao, B. Xu, Z. Liu, H. J. Snaith, N.-G. Park and W. Chen, *Nature*, 2024, **632**, 536–542.
6 C. Liu, Y. Yang, H. Chen, I. Spanopoulos, A. S. R. Bati, I. W. Gilley, J. Chen, A. Maxwell, B. Vishal, R. P. Reynolds, T. E. Wiggins, Z. Wang, C. Huang, J. Fletcher, Y. Liu, L. X. Chen, S. De Wolf, B. Chen, D. Zheng, T. J. Marks, A. Facchetti, E. H. Sargent and M. G. Kanatzidis, *Nature*, 2024, **633**, 359–364.
7 K. Zhao, Q. Liu, L. Yao, C. Değer, J. Shen, X. Zhang, P. Shi, Y. Tian, Y. Luo, J. Xu, J. Zhou, D. Jin, S. Wang, W. Fan, S. Zhang, S. Chu, X. Wang, L. Tian, R. Liu, L. Zhang, I. Yavuz, H.-f. Wang, D. Yang, R. Wang and J. Xue, *Nature*, 2024, **632**, 301–306.
8 N. J. Jeon, J. H. Noh, Y. C. Kim, W. S. Yang, S. Ryu and S. I. Seok, *Nat. Mater.*, 2014, **13**, 897–903.
9 M. Saliba, T. Matsui, J.-Y. Seo, K. Domanski, J.-P. Correa-Baena, M. K. Nazeeruddin, S. M. Zakeeruddin, W. Tress, A. Abate, A. Hagfeldt and M. Grätzel, *Energy Environ. Sci.*, 2016, **9**, 1989–1997.
10 Q. Jiang, Y. Zhao, X. Zhang, X. Yang, Y. Chen, Z. Chu, Q. Ye, X. Li, Z. Yin and J. You, *Nat. Photonics.*, 2019, **13**, 460–466.
11 T. Liu, Y. Zong, Y. Zhou, M. Yang, Z. Li, O. S. Game, K. Zhu, R. Zhu, Q. Gong and N. P. Padture, *Chem. Mater.*, 2017, **29**, 3246–3250.
12 J. Burschka, N. Pellet, S.-J. Moon, R. Humphry-Baker, P. Gao, M. K. Nazeeruddin and M. Grätzel, *Nature*, 2013, **499**, 316–319.
13 X. Zheng, B. Chen, J. Dai, Y. Fang, Y. Bai, Y. Lin, H. Wei, X. C. Zeng and J. Huang, *Nat. Energy*, 2017, **2**, 17102.
14 Z. Ni, C. Bao, Y. Liu, Q. Jiang, W.-Q. Wu, S. Chen, X. Dai, B. Chen, B. Hartweg, Z. Yu, Z. Holman and J. Huang, *Science*, 2020, **367**, 1352–1358.
15 Z. Gozukara Karabag, A. Karabag, U. Gunes, X.-X. Gao, O. A. Syzgantseva, M. A. Syzgantseva, F. Varlioglu Yaylali, N. Shibayama, H. Kanda, A. I. Rafieh, R. C. Turnell-Ritson, P. J. Dyson, S. Yerci, M. K. Nazeeruddin and G. Gunbas, *Adv. Energy Mater.*, 2023, **13**, 2302038.
16 G. Wu, R. Liang, M. Ge, G. Sun, Y. Zhang and G. Xing, *Adv. Mater.*, 2022, **34**, 2105635.
17 M. Li, Z. Zhu, Z. Wang, W. Pan, X. Cao, G. Wu and R. Chen, *Adv. Mater.*, 2024, **36**, 2309428.
18 B. Chen, P. N. Rudd, S. Yang, Y. Yuan and J. Huang, *Chem. Soc. Rev.*, 2019, **48**, 3842–3867.
19 J.-C. Blancon, J. Even, C. C. Stoumpos, M. G. Kanatzidis and A. D. Mohite, *Nat. Nanotechnol.*, 2020, **15**, 969–985.
20 S. You, F. T. Eickemeyer, J. Gao, J.-H. Yum, X. Zheng, D. Ren, M. Xia, R. Guo, Y. Rong, S. M. Zakeeruddin, K. Sivula, J. Tang, Z. Shen, X. Li and M. Grätzel, *Nat. Energy*, 2023, **8**, 515–525.
21 S. M. Park, M. Wei, J. Xu, H. R. Atapattu, F. T. Eickemeyer, K. Darabi, L. Grater, Y. Yang, C. Liu, S. Teale, B. Chen, H. Chen, T. Wang, L. Zeng, A. Maxwell, Z. Wang, K. R. Rao, Z. Cai, S. M. Zakeeruddin, J. T. Pham, C. M. Risko, A. Amassian, M. G. Kanatzidis, K. R. Graham, M. Grätzel and E. H. Sargent, *Science*, 2023, **381**, 209–215.
22 H. Chen, S. Teale, B. Chen, Y. Hou, L. Grater, T. Zhu, K. Bertens, S. M. Park, H. R. Atapattu, Y. Gao, M. Wei, A. K. Johnston, Q. Zhou, K. Xu, D. Yu, C. Han, T. Cui, E. H. Jung, C. Zhou, W. Zhou, A. H. Proppe, S. Hoogland, F. Laquai, T. Filleter, K. R. Graham, Z. Ning and E. H. Sargent, *Nat. Photonics*, 2022, **16**, 352–358.
23 N. Jiang, H.-W. Zhang, Y.-F. Liu, Y.-F. Wang, D. Yin and J. Feng, *Nano Lett.*, 2023, **23**, 6116–6123.
24 Y. Liang, F. Liu, X. Xie, Y. Ma, Y. Guan, W. Yu, Y. Zou, L. Zhang, X. Zhang, Y. Zhang, B. Li, C. Wu, K. Jiang, L. Xiao, D. Zou and S. Zheng, *Adv. Funct. Mater.*, 2024, **34**, 2401257.
25 F. Li, X. Deng, Z. Shi, S. Wu, Z. Zeng, D. Wang, Y. Li, F. Qi, Z. Zhang, Z. Yang, S.-H. Jang, F. R. Lin, S. W. Tsang, X.-K. Chen and A. K. Y. Jen, *Nat. Photonics*, 2023, **17**, 478–484.
26 G. Xing, B. Wu, X. Wu, M. Li, B. Du, Q. Wei, J. Guo, E. K. L. Yeow, T. C. Sum and W. Huang, *Nat. Comm.*, 2017, **8**, 14558.
27 H.-S. Kim, S. H. Im and N.-G. Park, *J. Phy. Chem. C*, 2014, **118**, 5615–5625.